Journal of Alloys and Compounds 470 (2009) 306–310

Contents lists available at ScienceDirect

Journal of Alloys and Compounds

journal homepage: www.elsevier.com/locate/jallcom

Phase transition, structure and luminescence of Eu:YAG nanophosphors by co-precipitation method

J. Su[a,*], Q.L. Zhang[b], S.F. Shao[b], W.P. Liu[b], S.M. Wan[b], S.T. Yin[b]

[a] College of Math and Physics, Nanjing University of Information Science and Technology, Nanjing 210044, China
[b] Anhui Institute of Optics and Fine Mechanics, Chinese Academy of Sciences, Hefei 230031, China

ARTICLE INFO

Article history:
Received 9 December 2007
Accepted 16 February 2008
Available online 2 April 2008

Keywords:
Phosphors
Chemical synthesis
Phase transitions
Optical spectroscopy
Luminescence

ABSTRACT

The methods to synthesize Eu:YAG phosphor by co-precipitation method and solid-state synthesis were compared. The dynamic aspects of the phase transition of Eu:YAG precursor synthesized by co-precipitation method were studied by using X-ray diffraction, infrared and Raman spectroscopy. The results showed that the precursor transformed to pure-YAG phase at the sintering temperature of 900 °C without intermediate phases present. Transmission electron microscope for the precursor powders sintered at 900–1200 °C showed that the powders were well-dispersed and had average size about 50–100 nm.The fluorescence spectra showed that the Eu:YAG phosphors had strong photoluminescence. The luminescence properties of the sintered powders depend on the sintering temperature were also analyzed.

1. Introduction

Yttrium aluminum garnet $Y_3A_{15}O_{12}$ (YAG) has been widely used as a host for solid-state laser materials and phosphor. Eu^{3+}-doped YAG materials are promising phosphor candidates in cathode-ray tubes (CRTs), field emission display (FED), scintillation, vacuum fluorescent displays (VFDs) and electroluminescent (EL) [1–4]. For phosphor materials, the purity of the host and the homogeneity of doped ions, which associated with the preparation processes [5–9], would strongly affect their optical characteristics. Therefore, it is necessary to study its preparation processes in more detail.

In this paper, Eu:YAG nanophosphors were synthesized by co-precipitation method and solid-state reaction process. X-ray diffraction (XRD), fourier transform infrared spectroscopy (FT-IR) and Raman spectroscopy were used to analyze the conversion procedure from the precursor to poly-crystalline Eu:YAG. Additionally, the structure of Eu:YAG poly-crystalline powders and YAG single crystal were compared by their molecular vibration spectra. Transmission electron microscopy (TEM) and fluorescence spectroscopy were used to investigate the morphology and luminescence of Eu:YAG nanophosphors.

2. Experimental

2.1. Co-precipitation method

$Y(NO_3)_3$ and $Eu(NO_3)_3$ solutions were prepared by dissolving spectroscopic pure Y_2O_3, Eu_2O_3 in diluted nitric acid. $Al(NO_3)_3$ solution was obtained by dissolving (>99%) $Al(NO_3)_3{\cdot}9H_2O$ in de-ionized water. Aqueous solutions of $Y(NO_3)_3$, $Al(NO_3)_3$ and $Eu(NO_3)_3$ were mixed according to the chemical formula $Y_{2.97}Eu_{0.03}Al_5O_{12}$, then the mixed nitrate solution and the aqueous ammonia were dropped simultaneously to ammonia solution with initial pH 9.5 under vigorous stirring. The dropping rate was adjusted to keep pH value in the range of 8–9. The precipitate slurry was stirred sufficiently after the reaction. Then the precipitate was separated and washed with de-ionized water for several times to remove NH_4^+, NO_3^- and OH^- etc. After that, the precipitation was dried at 110 °C and was then ground and sintered at various temperatures for 3 h in air.

2.2. Solid-state reaction process

Spectroscopic pure Al_2O_3, Y_2O_3 and Eu_2O_3 powders were mixed according to the chemical formula $Y_{2.97}Eu_{0.03}Al_5O_{12}$ and milled sufficiently, and then the mixture was sintered at 1500 °C for 48 h in air.

2.3. Characterizations

Infrared (IR) spectra were recorded on a fourier transform infrared spectrometer (Nicolet MAGNA-IR 750, USA). Raman spectra were obtained on a Raman spectrometer (RAMALOG 6, USA) with the 514.5 nm line of Ar^+ laser as the excitation resource. The laser beam was vertical to the (1 1 1) plane of YAG single crystal. XRD patterns were characterized by a Philips X'pert PRO X-ray diffractometer with Cu Kα radiation. The morphology and microstructure of the sintered powders were observed by transmitted electron microscopy (H-800, Japan). The luminescences were measured by a Jobin-Yvon spectrophotometer (FLUOROLOG 3 TAU, France). All the experiments were performed at room temperature.

* Corresponding author. Tel.: +86 25 58731031; fax: +86 25 58731174.
E-mail address: zlj007@126.com (J. Su).

0925-8388/$ – see front matter © 2008 Elsevier B.V. All rights reserved.
doi:10.1016/j.jallcom.2008.02.045

3. Results and discussion

3.1. Phase transition of Eu:YAG precursor

Fig. 1 shows the XRD spectra of the samples sintered at different temperatures. For the sample prepared by co-precipitation method, no obvious diffraction peak appeared at 800 °C, indicating that the powder is amorphous. At 900 °C, strong characteristic diffraction peaks of YAG (JCPD Card No. 33-40) were observed because the precursor converted to YAG poly-crystalline. No other intermediate phases were detected, which also indicates that no other intermediate phases, such as $YAlO_3$ (YAP, JCPD Card No. 33-41), $Y_4Al_2O_9$ (YAM, JCPD Card No. 34-368) occurred. Above 900 °C, continued refinement in peak shapes and intensities were observed because of the higher crystallization of the poly-crystalline. However, for the sample prepared by solid-state synthesis, YAP, YAM and Y_2O_3 phases still co-existed in YAG phase even if the reactants had been sintered at 1500 °C for 48 h. It indicates that co-precipitation method has advantage of lower synthesis temperature and shorter sintering time compared with solid-state synthesis.

Fig. 2 shows the FT-IR spectra of the precursor powder sintered at 900 °C and 1500 °C, respectively. The wide band at 3444 cm^{-1} and the weak band at 1639 cm^{-1} are assigned to O–H stretch and bend vibrations of the absorbed water. The bands at 787 cm^{-1}, 723 cm^{-1}, 690 cm^{-1}, 567 cm^{-1}, 511 cm^{-1} and 455 cm^{-1} are characteristic M–O vibrations of garnet crystals [10]. With the increase of the sintering temperature, the peaks had no apparent shift and became much sharper because of the higher crystallization.

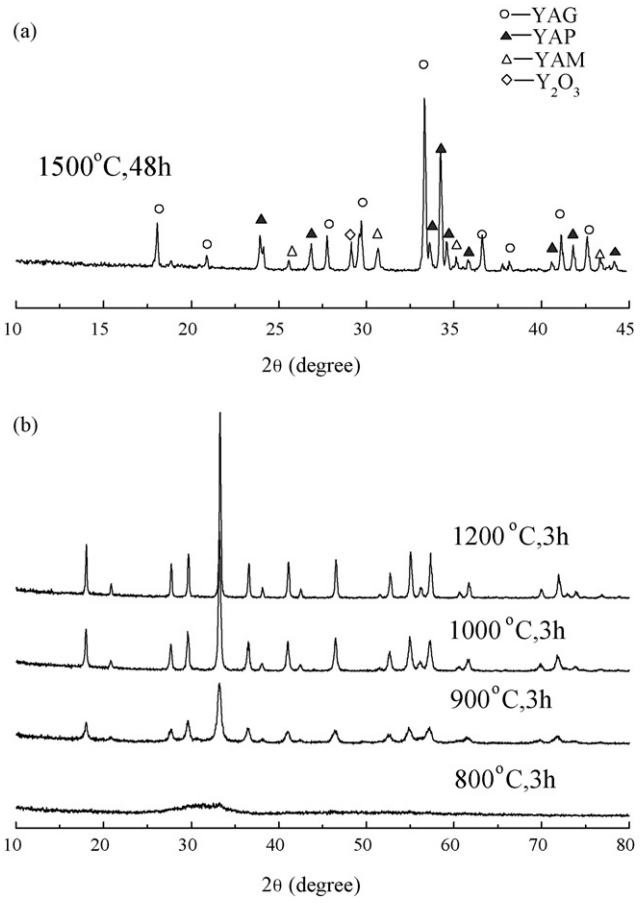

Fig. 1. XRD patterns of the powder synthesized by solid-state reaction method (a) and the powders sintered at different temperatures by co-precipitation method (b).

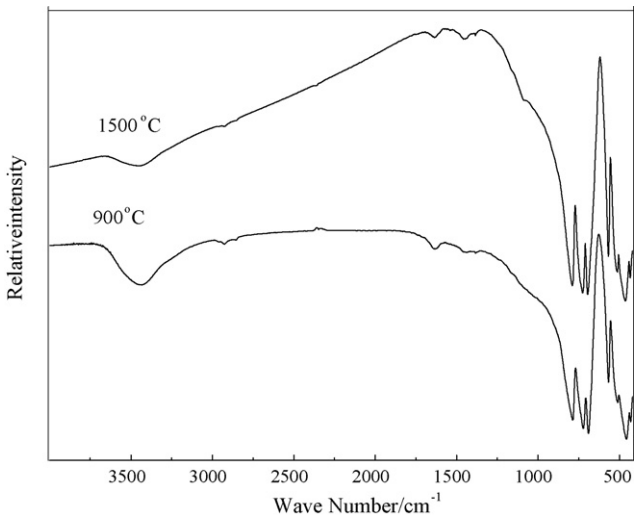

Fig. 2. FT-IR spectra of the Eu:YAG precursor powders sintered at 900 °C and 1500 °C.

Fig. 3a–d shows the Raman spectra of 1 at.%Eu:YAG precursor and the samples sintered at different temperatures for 3 h. Distinct changes in spectral shape present for the precursor and the powder sintered at different temperatures. For the precursor (Fig. 3a), the sharp strong band at 1048 cm^{-1} is associated with NO_3^-. The Raman spectra of the sample sintered at 800 °C presented weak broad Raman bands, corresponding to the amorphous sample. Characteristic garnet phase peaks were observed for the sample sintered at 1000 °C. By increasing the sintering temperature to 1500 °C, the intensities of the peaks increased and no distinct changes in the modes were observed, which suggested the powder had formed stable YAG garnet structure. Raman spectra of the powders sintered at 1000 °C (Fig. 3c) and 1500 °C (Fig. 3d) and YAG single crystal (Fig. 3e) were compared, almost all the peaks revealed identical band frequencies, which indicated that the Eu^{3+} substituted Y^{3+} and the structure of Eu:YAG was equivalent to YAG single crystal. The band at 478 cm^{-1} present in the Raman spectra of Eu:YAG nanocrystalline powder. However, it was absent in the spectra of YAG single crystal. According to the theoretical rigid ion model calculation of the rare earth aluminum garnets ($RE_3Al_5O_{12}$) by Papagelis et al. [11], the band at 478 cm^{-1} is associated with T_{2g} symmetry, and it was also absent in their experimental spectra. Additionally, the relatively intensity of the band at 748 cm^{-1} associated with E_g symmetry in Eu:YAG nanocrystalline powder was much stronger than that in YAG crystal. For the RE^{3+}-doped garnet material, the chief effect factors for the displacement activity are radius, valence and electronegativity. The radius of Eu^{3+} (0.113 nm) is larger than that of Y^{3+} (0.106nm), which could cause the lattice distortion. As a result, the intensity of T_{2g} and E_g modes in Eu:YAG powders increased.

3.2. Morphology of Eu:YAG nanophosphors

Fig. 4 shows the TEM micrographs of the precursor sintered at 900 °C and 1200 °C for 3 h. Both of the samples exhibited good dispersion. The particles sintered at 1200 °C were larger than that at 900 °C, which was mainly due to a higher crystalline after sintering at a higher temperature. It was estimated the diameters of spherical particles were smaller than 50 nm for the powder sin-

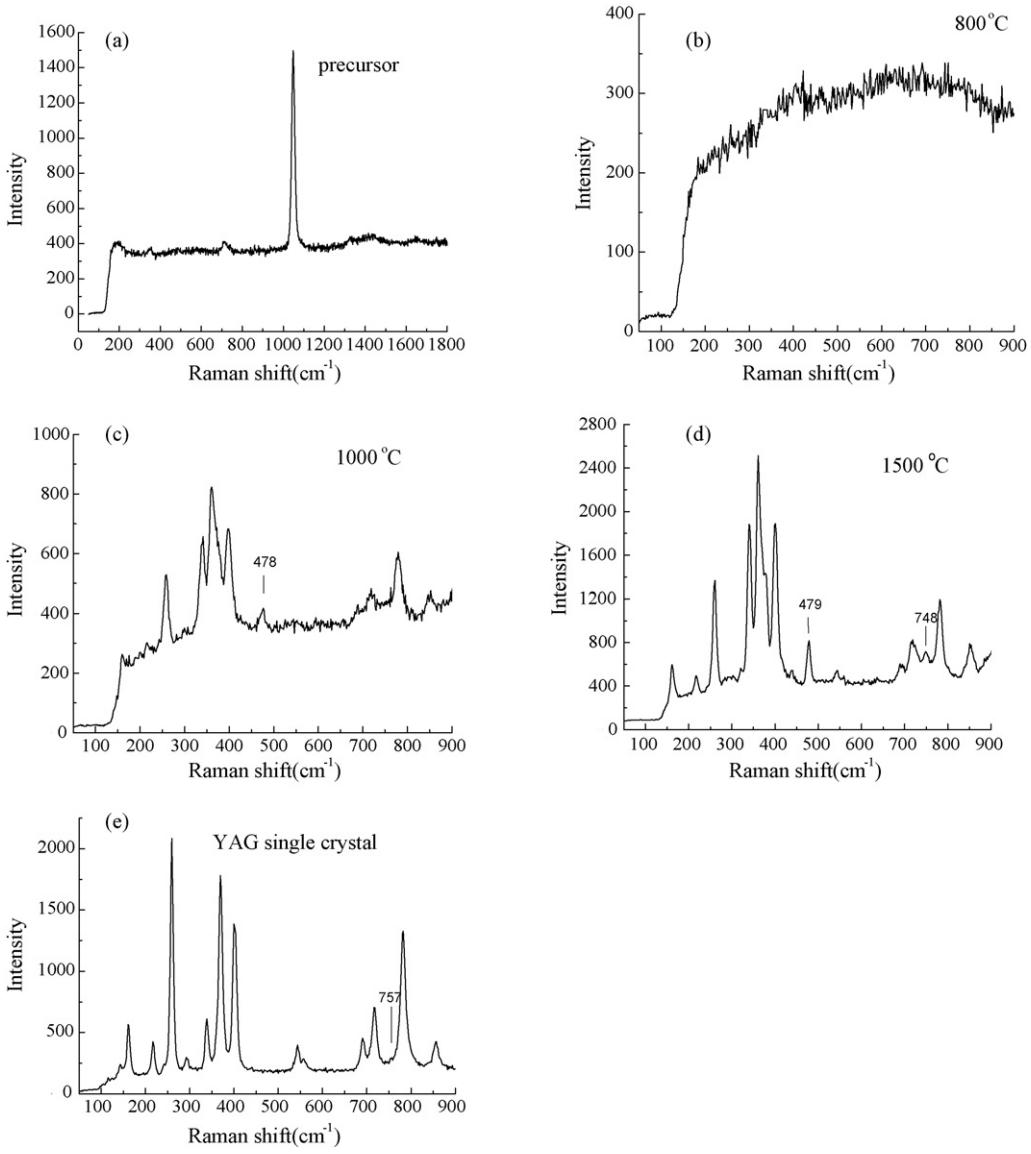

Fig. 3. Raman spectra of Eu:YAG precursor (a), the powder sintered at 800 °C (b), 1000 °C (c), 1500 °C (d) and YAG single crystal (e).

tered at 900 °C and were about 100 nm for the powder sintered at 1200 °C.

3.3. Luminescence properties

Fig. 5 shows the excitation spectra of the powders sintered at different temperatures by monitoring the emission at 590 nm. The bands in longer wave number region are corresponding to the f–f transitions within Eu^{3+} $4f^6$ configuration, the most prominent group at 394 nm is associated with $^7F_0$–$^5L_6$ transition. The broad band in the lower wave number region is associated with the charge transfer band (CTB) of Eu^{3+}–O^{2-}. For the powder sintered at 800 °C, the CTB of Eu^{3+} has a half width of 45 nm and a maximum at 270 nm. For the powders sintered at 1000 °C, the CTB

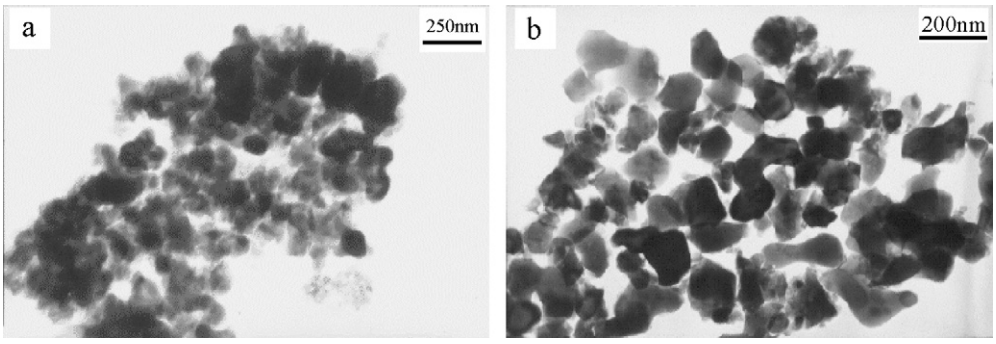

Fig. 4. TEM morphologies of YAG powders sintered at different temperatures (a) 900 °C and (b) 1200 °C.

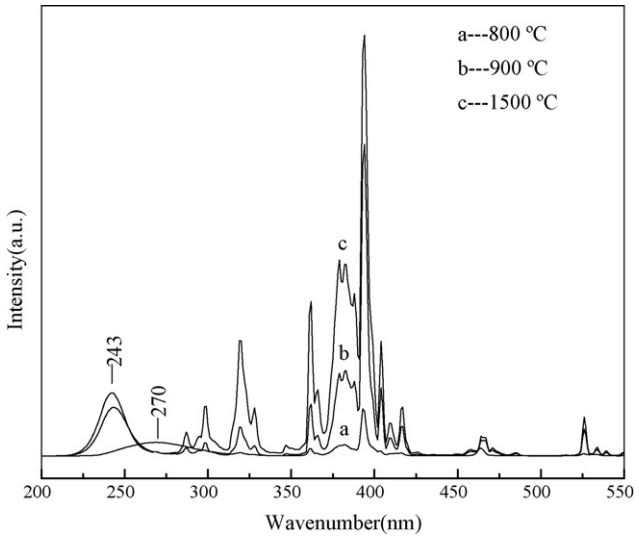

Fig. 5. Excitation spectra of the powders sintered at 800 °C, 1000 °C and 1500 °C (λ_{em} = 590 nm).

of Eu^{3+} is at 243 nm and has a half width of 19 nm.The spectra of the powders sintered at 1500 °C showed a higher intensity compared with that at 1000 °C, which should be associated with a higher crystallinity.

The emission spectrum excited upon 394 nm light is shown in Fig. 6. For the powders sintered at 1000 °C and 1500 °C (Fig. 6b), the spectra were composed of several sharp bands, which belong to the intrinsic emission of Eu^{3+}. The strongest band at 590 nm is ascribed to the Eu^{3+} magnetic dipole transition $^5D_0 \rightarrow {}^7F_1$. The 608 nm attributed to Eu^{3+} electric dipole transition $^5D_0 \rightarrow {}^7F_2$ is relatively weak. However, for the powder sintered at 800 °C, the Eu^{3+} electric dipole transition $^5D_0 \rightarrow {}^7F_2$ at 612 nm had stronger intensity compared with that of $^5D_0 \rightarrow {}^7F_1$ at 589 nm. It is due to that the magnetic dipole transition $^5D_0 \rightarrow {}^7F_1$ is not sensitive to the changes in the neighborhood of the Eu^{3+} ion while the electric dipole transition $^5D_0 \rightarrow {}^7F_2$ is very sensitive to any structural change [12–14]. Additionally, for the powder sintered at 800 °C, $^5D_0 \rightarrow {}^7F_0$ electric dipole transition at 579 nm was observed, but it was absent for the powders sintered at 1000 °C and 1500 °C. XRD and Raman analysis above suggest that the powder sintered at 800 °C is amorphous, indicating that most of the Eu^{3+} irons are located at the sites without inversion symmetry and the site symmetry of Eu^{3+} maybe C_s, C_n and C_{nv} [5,15]. As a result, the parity selection rules were broken and $^5D_0 \rightarrow {}^7F_0$ electric dipole transition at 579 nm present.

For the sample sintered at 1000 °C and 1500 °C, no changes were observed in the excitation and emission spectra except for the intensity. It indicated YAG garnet structure formed and the doped Eu^{3+} substituted for 8-coordinated Y^{3+} with site symmetry D_2, and the exact local symmetry is only a small distortion of the centrosymmetric D_{2h} point symmetry [2], according with our Raman spectra analysis. As a result, their luminescent intensity was concentrated mainly in the $^5D_0 \rightarrow {}^7F_1$ magnetic dipole transition rather than $^5D_0 \rightarrow {}^7F_2$ forced electric dipole transition.

For the powder sintered at 800 °C, the emission spectra excited upon 270 nm were shown in Fig. 6c, which had the same profile as that excited upon 394 (Fig. 6a). The results indicated that phosphor could be excited upon CTB of Eu^{3+}–O^{2-} and the f–f transition.

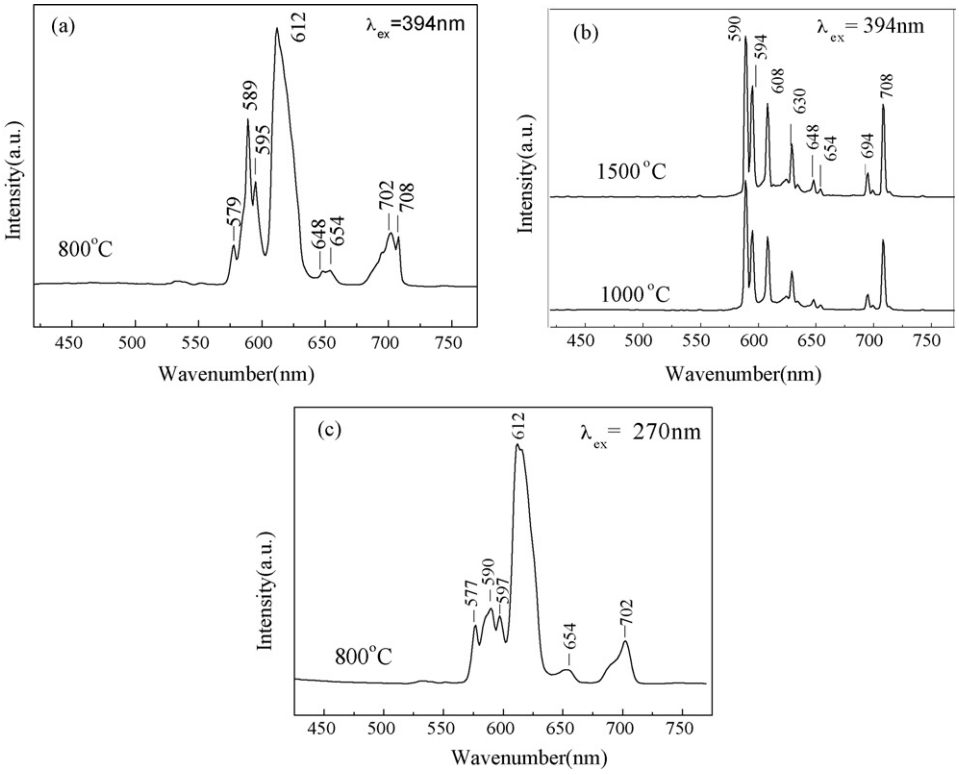

Fig. 6. Emission spectra of the powders sintered at 800 °C (a and c), 1000 °C and 1500 °C (b).

4. Conclusions

Eu:YAG precursor was synthesized successfully by co-precipitation method from nitrate solutions with NH_4OH as the precipitant. Co-precipitation method made the materials react uniformly at molecular level, and at lower temperature and for shorter sintering time. Experiments showed that the precursor transformed to YAG phase with no intermediate phases occurred. Eu:YAG nanophosphor particles could be obtained in the sintering temperature range of 900–1200 °C, and the lattice structure of Eu:YAG was a small distortion to YAG single crystal. The florescence spectra showed that the phosphor had good luminescence, and could be excited upon CTB of Eu^{3+}–O^{2-} and the f–f transition.

Prime novelty statement

The preparation processes were studied in more detail. The phase transition and structure information of the synthesized powders were analyzed by Raman spectra.

Acknowledgement

This work is financially supported by a grant from National Natural Science Foundation of China (No. 50472104).

References

[1] M.S. Scholl, J.R. Trimmer, J. Electrochem. Soc. 133 (1986) 643.
[2] D. Ravichandran, R. Roy, A.-G. Chakhovskoib, C.E. Hunt, W.B. White, S. Erdei, J. Lumin. 71 (1997) 291.
[3] S.K. Ruan, J.G. Zhou, A.M. Zhong, J.F. Duan, X.B. Yang, M.Z. Su, J. Alloys Compd. 72 (1998) 275.
[4] Y.C. Kang, I.W. Lenggoro, S.B. Park, K. Okuyama, J. Phys. Chem. Solids 60 (1999) 1855.
[5] Y.H. Zhou, J. Lin, S.B. Wang, H.J. Zhang, Opt. Mater. 20 (2002) 13.
[6] Y.H. Zhou, J. Lin, M. Yu, S.M. Han, S.B. Wang, H.J. Zhang, Mater. Res. Bull. 38 (2003) 12.
[7] C.H. Lu, W.T. Hsu, J. Dhanaraj, R. Jagannathan, J. Eur. Ceram. Soc. 24 (2004) 3723.
[8] G. Xia, S. Zhou, J. Zhang, S. Wang, Y. Liu, J. Xu, J. Cryst. Growth 283 (2005) 257.
[9] S. Georgescu, A.M. Chinie, A. Stefan, O. Toma, J. Optoelectron. Adv. Mater. 7 (2005) 2985.
[10] W.S. Peng, G.K. Liu, Infrared Spectra of Minerals, Science Press, Beijing, 1982 (in Chinese).
[11] K. Papagelis, G. Kanellis, S. Ves, G.A. Kourouklis, Phys. Stat. Sol. (b) 233 (2002) 134.
[12] C.K. Jogensen, B.R. Judd, Mol. Phys. 8 (1964) 281.
[13] R.D. Peacock, Struct. Bonding 22 (1975) 83.
[14] S. Georgescu, A.M. Chinie, A. Stefan, O. Toma, Phys. Stat. Sol. (c) 4 (2007) 946.
[15] G. Blasse, A. Bril, Philips Res. Rep. 2 (1966) 368.